

# Kinetic Blockade and Filamentary Pair Density Waves in Strain-Engineered Graphene

Tao Zhou<sup>1,2\*</sup>

<sup>1</sup>Guangdong Basic Research Center of Excellence for Structure and Fundamental Interactions of Matter,

Guangdong Provincial Key Laboratory of Quantum Engineering and Quantum Materials,

School of Physics, South China Normal University, Guangzhou 510006, China

<sup>2</sup>Guangdong-Hong Kong Joint Laboratory of Quantum Matter,

Frontier Research Institute for Physics, South China Normal University, Guangzhou 510006, China

We investigate superconductivity in strain-engineered graphene using a self-consistent Bogoliubov-de Gennes approach. Challenging the paradigm that the high density of states in flat bands universally enhances pairing, we identify a “kinetic blockade” mechanism: strain-induced sublattice polarization segregates electronic states, rendering these singularities inert. Instead, superconductivity emerges as robust filaments at geometric nodes, forming a pair density wave. This state features a sign-reversing order parameter, detectable via impurity-induced zero-energy modes. Our findings reveal a unique geometric origin for filamentary superconductivity, offering new perspectives on strain-tuned quantum phases in Dirac materials.

Since the isolation of graphene, realizing intrinsic superconductivity has been a central goal in condensed matter physics. The primary obstacle is the vanishing density of states (DOS) at the Dirac point. Early strategies primarily focused on extrinsic modifications, such as heavy chemical doping [1–3], substrate interaction [4], or proximity-induced pairing [5–7], which, while effective, inherently alter or mask the pristine nature of the carbon lattice.

A paradigm shift occurred recently with the rise of crystalline engineering in multilayer systems. Remarkable superconductivity has been achieved in Bernal-stacked bilayer graphene [8, 9], rhombohedral trilayer graphene [10], and most notably, magic-angle twisted bilayer and trilayer graphene [11–17]. These breakthroughs share a common principle: manipulating interlayer stacking or twist angles to engineer the electronic structure. In magic-angle twisted systems, this approach leads to flat bands and van Hove singularities, which drive strong correlations and superconductivity.

However, structurally deformed graphene offers a fundamentally different geometric route [18, 19]. Unlike the aforementioned systems that rely on multi-layer stacking, strain-engineered systems can generate colossal pseudo-magnetic fields (PMF) and flat pseudo-Landau-levels (PLLs) directly in a single sheet [20–29]. While the electronic topology and valley-polarized transport in the normal state of these systems have been extensively studied [20–29], the nature of the superconducting ground state hosting these flat bands remains unexplored. This gap is particularly conspicuous given the intense current interest in flat-band superconductivity: strain-induced PLLs offer a pristine platform where kinetic blockade might ostensibly boost pairing strength, yet the microscopic interplay between non-uniform strain textures and Cooper pairing is unknown.

In this Letter, we address this open question by investigating the superconducting phase of periodically corrugated

graphene. Contrary to the conventional wisdom that high density of states in flat bands universally enhances pairing, we identify a competing mechanism we term “kinetic blockade”. This geometric effect—arising from strain-induced sublattice wavefunction segregation—severs the nearest-neighbor overlap and suppresses the local pairing amplitude in the flat-band regions, effectively decoupling these states from the pairing instability despite the high DOS. Consequently, the superconducting condensate is spatially expelled from the flat-band regions and confined to the geometric nodes, resulting in a filamentary pair density wave (PDW) state.

*Model.*—We consider a superconducting system with strain-modulated hopping. The normal state Hamiltonian is given by the tight-binding model:

$$H_N = - \sum_{\langle i,j \rangle, \sigma} t_{ij} c_{i\sigma}^\dagger c_{j\sigma} - \mu \sum_{i, \sigma} c_{i\sigma}^\dagger c_{i\sigma}, \quad (1)$$

where  $t_{ij}$  denotes the hopping integral between sites  $i$  and  $j$ ,  $\mu$  represents the chemical potential,  $c_{i\sigma}^\dagger$  and  $c_{i\sigma}$  are the creation and annihilation operators for an electron with spin  $\sigma$  at site  $i$ , respectively, and  $\langle i,j \rangle$  indicates summation over nearest-neighbor pairs.

The hopping integral is modulated by unidirectional strain, corresponding to a periodically corrugated structure along the  $x$ -direction while remaining uniform along  $y$ . The corrugation is modeled as a sinusoidal ripple:

$$z(x) = H \sin\left(\frac{2\pi x}{L}\right), \quad (2)$$

where  $H$  is the corrugation amplitude and  $L$  is its period along  $x$ .

The strain-renormalized hopping integral follows the form

$$t_{ij} = t_0 \exp\left[-\beta\left(\frac{d_{ij}}{a_0} - 1\right)\right], \quad (3)$$

where  $t_0$  is the unstrained nearest-neighbor hopping amplitude.  $\beta$  is the decay constant with  $\beta = 3.37$  [30, 31].

\* [tzhou@scnu.edu.cn](mailto:tzhou@scnu.edu.cn)

$d_{ij}$  denotes the strained distance between sites  $i$  and  $j$ , and  $a_0$  is the equilibrium carbon-carbon bond length in graphene.

In the superconducting state, we consider a phenomenological on-site attractive interaction  $V$ , which serves as a minimal model for conventional  $s$ -wave pairing. This choice allows us to isolate the geometric effects of the strain-induced gauge fields from the complexities of unconventional pairing symmetries. The Hamiltonian can be diagonalized through solving the BdG equation, with,

$$\sum_j \begin{pmatrix} -t_{ij} - \mu\delta_{ij} & \Delta_{ij}\delta_{ij} \\ \Delta_{ij}^*\delta_{ij} & t_{ij}^* + \mu\delta_{ij} \end{pmatrix} \begin{pmatrix} u_j^n \\ v_j^n \end{pmatrix} = E_n \begin{pmatrix} u_i^n \\ v_i^n \end{pmatrix}. \quad (4)$$

The superconducting order parameters at site  $i$  are determined self-consistently at finite temperature  $T$  via

$$\Delta_i = \frac{V}{2} \sum_n u_{i,n} v_{i,n}^* \tanh \left( \frac{E_n}{2T} \right), \quad (5)$$

where  $V$  denotes the attractive pairing interaction strength.

The local density of states (LDOS) at site  $i$  and energy  $E$  is computed by summing over all energy bands:

$$\rho_i(E) = \sum_n [ |u_{i,n}|^2 \delta(E - E_n) + |v_{i,n}|^2 \delta(E + E_n) ]. \quad (6)$$

For numerical calculation, the delta function is approximated by a Lorentzian broadening:

$$\delta(x) \approx \frac{1}{\pi} \frac{\Gamma}{x^2 + \Gamma^2}, \quad (7)$$

where  $\Gamma$  is a small broadening parameter representing finite lifetime effects.

In the following results, we consider a unidirectional corrugated modulation with a period of  $L = 500$  unit cells and a corrugation ratio  $r = h/L = 0.16$ , a value within experimental reach [32, 33]. We use the unstrained nearest-neighbor hopping  $t_0$  as the unit of energy. Other parameters are set as follows: pairing interaction strength  $V = 1.6$ , the temperature  $T = 10^{-5}$ , the chemical potential  $\mu = 0$ , and the spectral broadening  $\Gamma = 0.004$ .

*Normal State and Sublattice Polarization.*—Before elucidating the superconducting state, we first characterize the electronic landscape of the normal state. As illustrated in Fig. 1(a), the unidirectional corrugation breaks the translational symmetry, generating a periodic PMF. The resulting band structure [Fig. 1(b)] exhibits flat bands at the Fermi energy ( $E = 0$ ), corresponding to the  $n = 0$  PLLs. These flat bands originate from the low-energy Dirac points at the two inequivalent valleys,  $K$  and  $K'$ . A defining feature of these strain-induced states, distinct from those generated by real magnetic fields, is the locking of the valley degree of freedom to the sublattice: due to the opposite signs of the PMF at

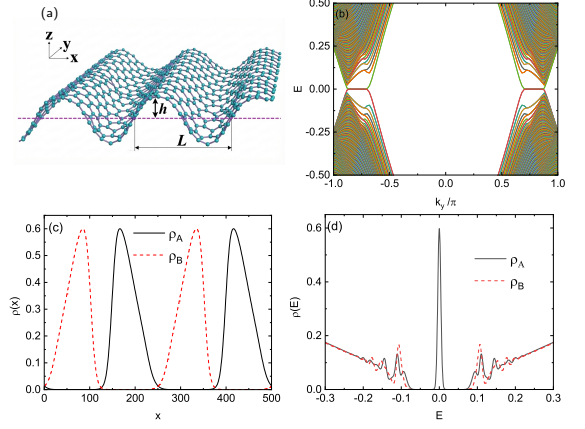


FIG. 1. Electronic structure of the corrugated graphene in the normal state. (a) Schematic illustration of the sinusoidally strain-engineered graphene lattice. (b) The calculated energy band structure along  $k_y$ , exhibiting flat bands at zero energy induced by the PMF. (c) Spatial profile of the zero-energy LDOS along the corrugated direction  $x$ . The solid (dashed) lines represent the A (B) sublattice, revealing a distinct spatial separation of the zeroth pseudo-Landau levels. (d) Energy-dependent LDOS at  $x = 0.33L$ , showing a sharp peak at the Fermi level for the A-sublattice (solid line) and a gap for the B-sublattice (dashed line).

the two valleys, the zeroth PLLs from the  $K$  valley localize exclusively on one sublattice, while those from the  $K'$  valley localize on the other.

This valley-dependent segregation is directly visualized in the zero-energy LDOS in Fig. 1(c): the wavefunctions are spatially separated, with A-sublattice states localized near  $x = 0.33L$  and  $0.83L$ , and B-sublattice states peaking at  $x = 0.17L$  and  $0.67L$ . This leads to a scenario where, locally, the high-DOS flat bands are hosted almost exclusively by a single sublattice [Fig. 1(d)]. This sublattice segregation is not merely a spectral feature but a fundamental obstruction to pairing, as we discuss below.

*Geometric Segregation of Superconductivity: Kinetic Blockade versus Strained Enhancement.*—We now turn to the self-consistent solution of the superconducting order parameter  $\Delta(x)$ . Fig. 2(a) plots the spatial profile of the order parameter amplitude  $|\Delta(x)|$ . A striking phenomenon is revealed that defies the conventional “flat-band superconductivity” paradigm: the pairing amplitude is not maximized in the high-DOS flat-band regions (marked by arrows). Instead, a spatial dissociation occurs—superconductivity is suppressed in the flat bands and re-emerges as robust filaments at nodes of corrugation ( $z = 0$ ).

We identify two competing geometric mechanisms driving this dissociation. First, and most prominently, the flat-band regions suffer from a kinetic blockade. Contrary to the conventional wisdom that high DOS enhances the pairing amplitude, we observe a suppression of  $\Delta$  in these regions. This suppression originates from the extreme sublattice polarization induced by the pseudo-

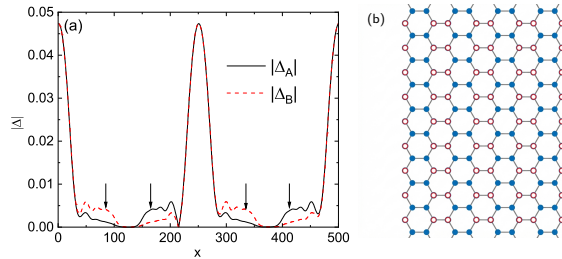


FIG. 2. Spatial dissociation of superconductivity and the emergence of a PDW. (a) Self-consistent profile of the superconducting order parameter amplitude  $|\Delta(x)|$  along the corrugation. The maximum pairing amplitude emerges at the geometric nodes, whereas the flat-band regions (marked by arrows) exhibit suppressed pairing despite the high DOS. (b) Schematic representation of the superconducting phase on the graphene lattice in the high- $\Delta$  region. The solid (blue) and hollow (red) circles represent sites with opposite signs of the order parameter ( $\pm$ ), illustrating the formation of a sign-reversing PDW state.

magnetic field, where the electronic density is confined to a single sublattice while vanishing on the other [Figs. 1(c) and 1(d)]. Such spatial segregation severs the nearest-neighbor wavefunction overlap. Consequently, the superconducting state inherits this polarization, manifesting as a marked asymmetry between the sublattice order parameters ( $|\Delta_A| \neq |\Delta_B|$ ), as evident in Fig. 2(a). Since the establishment of a coherent condensate requires kinetic mixing between sites to lower the free energy, this spatial disjointedness effectively decouples the localized flat-band states from the pairing instability, thereby nullifying the benefit of the divergent DOS.

Conversely, at the nodes of corrugation ( $z = 0$ ), the physics is governed by bond stretching rather than the PMF. Here, the vanishing pseudo-magnetic field ensures the restoration of A-B sublattice symmetry, facilitating the necessary wavefunction overlap. The maximal tensile strain exponentially suppresses the local hopping  $t_{ij}$  [Eq. (2)], thereby enhancing the effective correlation ratio  $V/t_{\text{eff}}$ . This drives the system locally into a strong-coupling regime. Unlike the fragile flat-band states, the electrons at the nodes retain sufficient A-B sublattice overlap to support robust phase coherence, resulting in the formation of quasi-one-dimensional superconducting filaments.

Additionally, we observe that  $\Delta_x$  vanishes at the crests and troughs ( $x = 0.25L$  and  $0.75L$ ). Although the A-B sublattice symmetry is fully recovered in these zero-PMF regions, the local slope of the sinusoidal corrugation profile  $z(x)$  [Eq. (2)] vanishes, meaning the lattice distortion is minimal. Consequently, the effective hopping  $t_{\text{eff}}$  relaxes back to the unstrained value  $t_0$ . Lacking both the flat bands and the strain-induced bandwidth narrowing, these regions effectively mimic pristine graphene, which remains in the weak-coupling limit and is non-superconducting at the simulated interaction strength.

*Mechanism of Time-Reversal-Invariant PDW.*—The

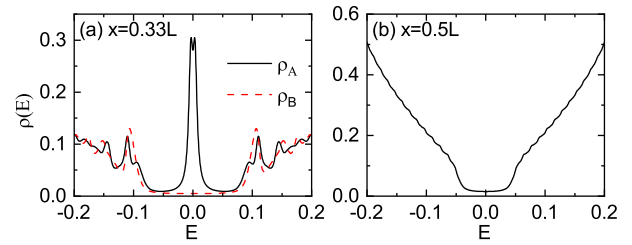


FIG. 3. LDOS in the superconducting state. (a) LDOS in the flat-band region ( $x = 0.33L$ ). The strong sublattice polarization persists (dashed vs. solid lines), but the original normal-state zero-energy peak is split, indicating the opening of a partial superconducting gap. (b) LDOS at the node of corrugation ( $x = 0.5L$ ), where the sublattice symmetry is restored.

emergence of the PDW state is a direct consequence of the strain-induced gauge potential coupling to the valley degrees of freedom ( $K$  and  $K'$ ). The spatial modulation of hopping integrals generates an effective vector potential  $\mathbf{A}(\mathbf{r})$ . Crucially, consistent with the valley-dependent physics discussed in the normal state, this strain-induced field is valley-contrasting, satisfying  $\mathbf{A}_K = -\mathbf{A}_{K'}$ , which preserves the global time-reversal symmetry (TRS). In this landscape, electrons at the  $K$  and  $K'$  valleys experience opposite gauge potentials. Consequently, Cooper pairs formed by time-reversal partners  $(K, \uparrow; K', \downarrow)$  acquire a finite center-of-mass momentum modulation to optimize their kinetic energy in the presence of the staggered field. Unlike the field-induced Fulde-Ferrell-Larkin-Ovchinnikov (FFLO) state driven by Zeeman splitting [34, 35], this state is driven by the orbital geometric phase. To satisfy the local phase constraints imposed by  $\mathbf{A}(\mathbf{r})$  while minimizing the free energy, the superconducting condensate develops a sign-reversing structure,  $\text{sgn}[\Delta(\mathbf{r})] = \pm 1$ . This spontaneous formation of a spatially oscillating order parameter with preserved TRS constitutes an intrinsic pair density wave.

*Spectral Signatures and Hard Gap.*—In the flat-band region ( $x=0.33L$ , Fig. 3a), the LDOS retains the strong sublattice polarization characteristic of the normal state, with the A and B sublattices remaining spectrally separated. However, a crucial change occurs: the sharp zero-energy peak observed in the normal state (Fig. 1d) is now split into two peaks centered away from the Fermi level. This splitting signifies the opening of a superconducting gap  $\Delta_{\text{flat}}$  on the flat bands. The persistence of sublattice separation implies that the Cooper pairs in this region are formed between electrons residing on distinct sublattices that are spatially segregated, confirming the “kinetic blockade” scenario where superconductivity is weakly coherent.

In stark contrast, at the nodes of corrugation ( $x = 0.5L$ , Fig. 3b), where the order parameter is maximized, the A and B sublattice spectra become identical, indicating a restoration of local sublattice symmetry. A large, hard gap is clearly visible, reflecting the robust pairing

amplitude in these quasi-one-dimensional filaments. Notably, the spectrum exhibits a striking absence of sharp coherence peaks at the gap edges, which are hallmarks of conventional BCS superconductivity. This suppression of coherence peaks is attributed to the combined effects of the intrinsic PDW texture and the strong-coupling nature of the superconductivity in these strained regions. The sign-reversing order parameter and the effective reduction of dimensionality (to quasi-1D filaments) redistribute the spectral weight, leading to a smooth gap profile rather than sharp pile-ups.

*Impurity-Induced Zero Modes as a Robust Sign-Reversal Probe.*—To provide a definitive experimental signature distinguishing the proposed PDW state from conventional *s*-wave superconductivity, we investigate the local electronic response to a single non-magnetic impurity. We introduce a localized impurity potential  $H_{\text{imp}} = V_i \sum_{\sigma} c_{0\sigma}^{\dagger} c_{0\sigma}$  at a site within the superconducting filament ( $x = 0.5L$ ) and calculate the LDOS at its nearest-neighbor site.

Fig. 4 displays the evolution of the LDOS spectra with increasing impurity strength  $V_i$ . In the clean limit ( $V_i = 0$ , cyan curve), the spectrum shows a hard gap consistent with the bulk superconducting state. As the non-magnetic scattering potential is turned on ( $V_i = 5, 10$ ), a spectral weight transfer occurs, leading to the emergence of a resonance peak inside the superconducting gap. In the unitary scattering limit ( $V_i = 100$ , black solid curve), which represents a strong scatterer or a vacancy, a sharp, pronounced peak forms at exactly zero energy ( $E = 0$ ).

This result is a direct manifestation of a general principle for the non-magnetic impurity effect: impurity-induced resonance is a universal and robust fingerprint of sign-reversing superconductivity [36, 37]. In Ref. [37], it has been demonstrated that the emergence of in-gap states is inextricably linked to the scattering of quasi-particles between electronic states with opposite pairing signs.

In the PDW state, the order parameter undergoes a spontaneous sign reversal between adjacent unit cells [Fig. 2(b)]. Consequently, a local impurity inevitably scatters electrons across this sign boundary, inducing the destructive interference required to form a bound state. The observation of such zero-bias conductance peaks in scanning tunneling microscopy (STM) would therefore serve as definitive evidence, clearly differentiating this intrinsic PDW state from a trivial proximity effect or uniform *s*-wave pairing.

*Remark on Pairing Symmetry.*—We employed an on-site attractive interaction, which corresponds to the standard *s*-wave pairing channel. While this interaction typically stabilizes a uniform, isotropic condensate in pristine graphene, our results demonstrate that the strain texture forces the system into a sign-changing PDW state. This implies that even the most robust pairing channel (*s*-wave) is vulnerable to the “kinetic blockade” mechanism. Since on-site singlets rely on inter-sublattice hopping to establish global coherence, the strain-induced seg-

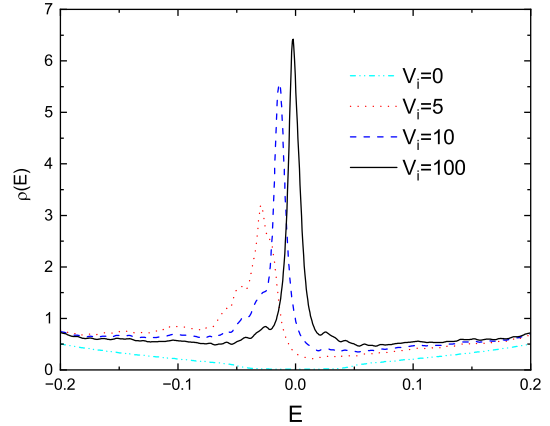


FIG. 4. Detection of the PDW state via non-magnetic impurity scattering. The LDOS at a nearest-neighbor site of a non-magnetic impurity located in the superconducting region is plotted for various impurity strengths  $V_i$ .

regation of A and B sublattices suppresses the uniform phase. This geometric obstruction would likely be even more detrimental to non-local pairing symmetries (e.g., *d*-wave) that rely explicitly on inter-site bonds.

*Experimental Feasibility.*—The periodic strain textures modeled here ( $L = 500$  unit cells, corrugation ratio  $r = 0.16$ ) are well within the reach of current strain-engineering capabilities. Large-amplitude corrugations and crumpled structures exceeding this aspect ratio have been realized by relaxing graphene on pre-stretched elastomeric substrates [32] or through kirigami-inspired mechanical manipulation [33]. These experiments demonstrate that monolayer graphene possesses exceptional mechanical resilience, sustaining high-curvature deformations without fracture. Consequently, these strain-engineered platforms provide an ideal arena to experimentally verify the predicted geometric dissociation of superconductivity and the associated PDW state.

*Broader Implications: Strain, Filaments, and Selectivity.*—Our findings offer a timely theoretical framework for interpreting the role of strain in correlated oxides, particularly the very recent realization of ambient-pressure superconductivity in  $\text{La}_3\text{Ni}_2\text{O}_7$  thin films [38, 39]. In these experiments, epitaxial strain serves as a critical tuning parameter, substituting for high pressure [40]. Notably, transport measurements suggest a possible filamentary origin or domain-wired character for the resulting superconductivity [39]. This phenomenology closely aligns with our prediction in corrugated graphene, where strain gradients drive a spatial dissociation of electronic states, confining superconductivity to specific geometric loci (nodes) while suppressing it elsewhere.

We propose that this “strain-induced filamentation” shares a phenomenological similarity across these distinct systems: the geometric disentanglement of internal degrees of freedom. In nickelates, the minimal model involves two active orbitals ( $d_{z^2}$  and  $d_{x^2-y^2}$ ); theoretical studies suggest superconductivity is mediated by

an orbital-selective mechanism [41–43]. Our corrugated graphene system presents a precise geometric dual: the two sublattices (A and B) play the role of the two orbitals. The “kinetic blockade” we identify is essentially a sublattice-selective localization. Just as strain can differentially tune orbital overlaps in nickelates, it spatially segregates sublattices in graphene. Our work thus suggests a generalized principle: non-uniform strain does not merely renormalize bandwidths but acts as a “phase filter,” spatially separating regions of coherent pairing (nodes) from regions of kinetic blockade (flat bands), naturally leading to the filamentary or textured superconductivity.

*Summary.*—In summary, we have demonstrated that

structurally corrugated graphene provides a geometric platform for unconventional superconductivity, distinct from the twistronics paradigm. We identified a “kinetic blockade” mechanism that suppresses pairing in flat bands due to sublattice polarization, while strain-enhanced coupling drives robust, filamentary superconductivity at the nodes. The resulting state is a time-reversal-invariant PDW, detectable via impurity-induced zero-energy modes. These findings not only uncover a new phase in Dirac materials but also underscore the universality of strain engineering, providing a theoretical basis for understanding the emergent filamentary superconductivity recently observed in epitaxial nickelate films.

---

[1] S. Ichinokura, K. Sugawara, A. Takayama, T. Takahashi, and S. Hasegawa, Superconducting calcium-intercalated bilayer graphene, *ACS Nano* **10**, 2761 (2016).

[2] J. Chapman, Y. Su, C. A. Howard, D. Kundys, A. N. Grigorenko, F. Guinea, A. K. Geim, I. V. Grigorieva, and R. R. Nair, Superconductivity in ca-doped graphene laminates, *Sci. Rep.* **6**, 23254 (2016).

[3] B. M. Ludbrook, G. Levy, P. Nigge, M. Zonno, M. Schneider, D. J. Dvorak, C. N. Veenstra, S. Zhdanovich, D. Wong, P. Dosanjh, C. Straßer, A. Stöhr, S. Forti, C. R. Ast, U. Starke, and A. Damascelli, Evidence for superconductivity in li-decorated monolayer graphene, *Proc. Natl. Acad. Sci. U. S. A.* **112**, 11795 (2015).

[4] C. Tonnour, A. Kimouche, J. Coraux, L. Magaud, B. Delsol, B. Gilles, and C. Chapelier, Induced superconductivity in graphene grown on rhenium, *Phys. Rev. Lett.* **111**, 246805 (2013).

[5] A. Di Bernardo, O. Millo, M. Barbone, H. Alpern, Y. Kalcheim, U. Sassi, A. K. Ott, D. De Fazio, D. Yoon, M. Amado, A. C. Ferrari, J. Linder, and J. W. A. Robinson, p-wave triggered superconductivity in single-layer graphene on an electron-doped oxide superconductor, *Nat. Commun.* **8**, 14024 (2017).

[6] G.-H. Lee and H.-J. Lee, Proximity coupling in superconductor-graphene heterostructures, *Rep. Prog. Phys.* **81**, 056502 (2018).

[7] E. Cortés-del Río, J. L. Lado, V. Cherkez, P. Mallet, J.-Y. Veuillet, J. C. Cuevas, J. M. Gómez-Rodríguez, J. Fernández-Rossier, and I. Brihuega, Observation of yu-shiba-rusinov states in superconducting graphene, *Adv. Mater.* **33**, 2008113 (2021).

[8] H. Zhou, L. Holleis, Y. Saito, L. Cohen, W. Huynh, C. L. Patterson, F. Yang, T. Taniguchi, K. Watanabe, and A. F. Young, Isospin magnetism and spin-polarized superconductivity in bernal bilayer graphene, *Science* **375**, 774 (2022).

[9] Y. Zhang, R. Polski, A. Thomson, É. Lantagne-Hurtubise, C. Lewandowski, H. Zhou, K. Watanabe, T. Taniguchi, J. Alicea, and S. Nadj-Perge, Enhanced superconductivity in spin-orbit proximitized bilayer graphene, *Nature* **613**, 268 (2023).

[10] H. Zhou, T. Xie, T. Taniguchi, K. Watanabe, and A. F. Young, Superconductivity in rhombohedral trilayer graphene, *Nature* **598**, 434 (2021).

[11] Y. Cao, V. Fatemi, S. Fang, K. Watanabe, T. Taniguchi, E. Kaxiras, and P. Jarillo-Herrero, Unconventional superconductivity in magic-angle graphene superlattices, *Nature* **556**, 43 (2018).

[12] Y. Cao, J. M. Park, K. Watanabe, T. Taniguchi, and P. Jarillo-Herrero, Pauli-limit violation and re-entrant superconductivity in moiré graphene, *Nature* **595**, 526 (2021).

[13] J. M. Park, Y. Cao, K. Watanabe, T. Taniguchi, and P. Jarillo-Herrero, Tunable strongly coupled superconductivity in magic-angle twisted trilayer graphene, *Nature* **590**, 249 (2021).

[14] J. M. Park, Y. Cao, L.-Q. Xia, S. Sun, K. Watanabe, T. Taniguchi, and P. Jarillo-Herrero, Robust superconductivity in magic-angle multilayer graphene family, *Nat. Mater.* **21**, 877 (2022).

[15] Y. Zhang, R. Polski, C. Lewandowski, A. Thomson, Y. Peng, Y. Choi, H. Kim, K. Watanabe, T. Taniguchi, J. Alicea, F. von Oppen, G. Refael, and S. Nadj-Perge, Promotion of superconductivity in magic-angle graphene multilayers, *Science* **377**, 1538 (2022).

[16] Z. Hao, A. M. Zimmerman, P. Ledwith, E. Khalaf, D. H. Najafabadi, K. Watanabe, T. Taniguchi, A. Vishwanath, and P. Kim, Electric field-tunable superconductivity in alternating-twist magic-angle trilayer graphene, *Science* **371**, 1133 (2021).

[17] J. M. Park, S. Sun, K. Watanabe, T. Taniguchi, and P. Jarillo-Herrero, Experimental evidence for nodal superconducting gap in moiré graphene, *Science* **391**, 79 (2026).

[18] J. C. Meyer, A. K. Geim, M. I. Katsnelson, K. S. Novoselov, T. J. Booth, and S. Roth, The structure of suspended graphene sheets, *Nature* **446**, 60 (2007).

[19] A. Fasolino, J. H. Los, and M. I. Katsnelson, Intrinsic ripples in graphene, *Nat. Mater.* **6**, 858 (2007).

[20] M. M. Fogler, F. Guinea, and M. I. Katsnelson, Pseudomagnetic fields and ballistic transport in a suspended graphene sheet, *Phys. Rev. Lett.* **101**, 226804 (2008).

[21] F. Guinea, M. I. Katsnelson, and M. A. H. Vozmediano, Midgap states and charge inhomogeneities in corrugated graphene, *Phys. Rev. B* **77**, 075422 (2008).

[22] T. O. Wehling, A. V. Balatsky, A. M. Tsvelik, M. I. Katsnelson, and A. I. Lichtenstein, Midgap states in corrugated graphene: Ab initio calculations and effective field

theory, *Europhys. Lett.* **84**, 17003 (2008).

[23] S. Costamagna, O. Hernandez, and A. Dobry, Spectral gap induced by structural corrugation in armchair graphene nanoribbons, *Phys. Rev. B* **81**, 115421 (2010).

[24] M. Vozmediano, M. Katsnelson, and F. Guinea, Gauge fields in graphene, *Phys. Rep.* **496**, 109 (2010).

[25] F. Guinea, M. I. Katsnelson, and A. K. Geim, Energy gaps and a zero-field quantum hall effect in graphene by strain engineering, *Nat. Phys.* **6**, 30 (2010).

[26] L. Meng, W.-Y. He, H. Zheng, M. Liu, H. Yan, W. Yan, Z.-D. Chu, K. Bai, R.-F. Dou, Y. Zhang, Z. Liu, J.-C. Nie, and L. He, Strain-induced one-dimensional landau level quantization in corrugated graphene, *Phys. Rev. B* **87**, 205405 (2013).

[27] J. Xu, Z. Zhang, and P. Cui, Coexistence and interplay of pseudomagnetism and flexoelectricity in few-layer rippled graphene, *npj Quantum Mater.* **9**, 102 (2024).

[28] S.-Y. Li, K.-K. Bai, L.-J. Yin, J.-B. Qiao, W.-X. Wang, and L. He, Observation of unconventional splitting of landau levels in strained graphene, *Phys. Rev. B* **92**, 245302 (2015).

[29] Y.-W. Liu, Z. Zhan, Z. Wu, C. Yan, S. Yuan, and L. He, Realizing one-dimensional electronic states in graphene via coupled zeroth pseudo-landau levels, *Phys. Rev. Lett.* **129**, 056803 (2022).

[30] V. M. Pereira, A. H. Castro Neto, and N. M. R. Peres, Tight-binding approach to uniaxial strain in graphene, *Phys. Rev. B* **80**, 045401 (2009).

[31] S.-M. Choi, S.-H. Jhi, and Y.-W. Son, Effects of strain on electronic properties of graphene, *Phys. Rev. B* **81**, 081407 (2010).

[32] J. Zang, S. Ryu, N. Pugno, Q. Wang, Q. Tu, M. J. Buehler, and X. Zhao, Multifunctionality and control of the crumpling and unfolding of large-area graphene, *Nat. Mater.* **12**, 321 (2013).

[33] M. K. Blees, A. W. Barnard, P. A. Rose, S. P. Roberts, K. L. McGill, P. Y. Huang, A. R. Ruyack, J. W. Kevek, B. Kobrin, D. A. Muller, and P. L. McEuen, Graphene kirigami, *Nature* **524**, 204 (2015).

[34] P. Fulde and R. A. Ferrell, Superconductivity in a strong spin-exchange field, *Phys. Rev.* **135**, A550 (1964).

[35] A. I. Larkin and Y. N. Ovchinnikov, Nonuniform state of superconductors, *Sov. Phys. JETP* **20**, 762 (1965).

[36] A. V. Balatsky, I. Vekhter, and J.-X. Zhu, Impurity-induced states in conventional and unconventional superconductors, *Rev. Mod. Phys.* **78**, 373 (2006).

[37] J. Huang, Z. D. Wang, and T. Zhou, Probing sign-changing order parameters via impurity states in unconventional superconductors: Implications for  $\text{La}_3\text{Ni}_2\text{O}_7$  superconductors with interlayer pairing, *Phys. Rev. B* **111**, 174525 (2025).

[38] G. Zhou, W. Lv, H. Wang, Z. Nie, Y. Chen, Y. Li, H. Huang, W.-Q. Chen, Y.-J. Sun, Q.-K. Xue, and Z. Chen, Ambient-pressure superconductivity onset above 40 K in  $(\text{La},\text{Pr})_3\text{Ni}_2\text{O}_7$  films, *Nature* **640**, 641 (2025).

[39] E. K. Ko, Y. Yu, Y. Liu, L. Bhatt, J. Li, V. Thampy, C.-T. Kuo, B. Y. Wang, Y. Lee, K. Lee, J.-S. Lee, B. H. Goodge, D. A. Muller, and H. Y. Hwang, Signatures of ambient pressure superconductivity in thin film  $\text{La}_3\text{Ni}_2\text{O}_7$ , *Nature* **638**, 935 (2025).

[40] H. Sun, M. Huo, X. Hu, J. Li, Z. Liu, Y. Han, L. Tang, Z. Mao, P. Yang, B. Wang, J. Cheng, D.-X. Yao, G.-M. Zhang, and M. Wang, Signatures of superconductivity near 80 K in a nickelate under high pressure, *Nature* **621**, 493–498 (2023).

[41] Z. Luo, X. Hu, M. Wang, W. Wú, and D.-X. Yao, Bilayer two-orbital model of  $\text{La}_3\text{Ni}_2\text{O}_7$  under pressure, *Phys. Rev. Lett.* **131**, 126001 (2023).

[42] J. Chen, F. Yang, and W. Li, Orbital-selective superconductivity in the pressurized bilayer nickelate  $\text{La}_3\text{Ni}_2\text{O}_7$ : An infinite projected entangled-pair state study, *Phys. Rev. B* **110**, L041111 (2024).

[43] J. Huang and T. Zhou, Effective perpendicular electric field as a probe for interlayer pairing in ambient-pressure superconducting  $\text{La}_{2.85}\text{Pr}_{0.15}\text{Ni}_2\text{O}_7$  thin films, *Phys. Rev. B* **112**, 054506 (2025).